

Event-Enhanced Multi-Modal Spiking Neural Network for Dynamic Obstacle Avoidance

Yang Wang
Dalian University of Technology
Dalian, China
yangwang06@mail.dlut.edu.cn

Bo Dong
Princeton University
Princeton, USA
bo.dong@princeton.edu

Yuji Zhang
Dalian University of Technology
Dalian, China
yujizhang@mail.dlut.edu.cn

Yunduo Zhou
Dalian University of Technology
Dalian, China
1227627334@mail.dlut.edu.cn

Haiyang Mei
Dalian University of Technology &
National University of Singapore
Dalian, China
haiyang.mei@outlook.com

Ziqi Wei
Institute of Automation, Chinese
Academy of Sciences & Dalian
University of Technology
Beijing, China
ziqi.wei@ia.ac.cn

Xin Yang*
Dalian University of Technology
Dalian, China
xinyang@dlut.edu.cn

ABSTRACT

Autonomous obstacle avoidance is of vital importance for an intelligent agent such as a mobile robot to navigate in its environment. Existing state-of-the-art methods train a spiking neural network (SNN) with deep reinforcement learning (DRL) to achieve energy-efficient and fast inference speed in complex/unknown scenes. These methods typically assume that the environment is static while the obstacles in real-world scenes are often *dynamic*. The movement of obstacles increases the complexity of the environment and poses a great challenge to the existing methods. In this work, we approach robust dynamic obstacle avoidance twofold. First, we introduce the neuromorphic vision sensor (*i.e.*, event camera) to provide *motion cues* complementary to the traditional Laser depth data for handling dynamic obstacles. Second, we develop an DRL-based event-enhanced multimodal spiking actor network (EEM-SAN) that extracts information from motion events data via *unsupervised representation learning* and fuses Laser and event camera data with *learnable thresholding*. Experiments demonstrate that our EEM-SAN outperforms state-of-the-art obstacle avoidance methods by a significant margin, especially for dynamic obstacle avoidance.

CCS CONCEPTS

• **Computing methodologies** → **Vision for robotics; Reinforcement learning; Spiking neural networks.**

*Corresponding author.

Permission to make digital or hard copies of all or part of this work for personal or classroom use is granted without fee provided that copies are not made or distributed for profit or commercial advantage and that copies bear this notice and the full citation on the first page. Copyrights for components of this work owned by others than the author(s) must be honored. Abstracting with credit is permitted. To copy otherwise, or republish, to post on servers or to redistribute to lists, requires prior specific permission and/or a fee. Request permissions from [permissions@acm.org](https://www.acm.org/permissions).

MM '23, October 29–November 3, 2023, Ottawa, ON, Canada

© 2023 Copyright held by the owner/author(s). Publication rights licensed to ACM.

ACM ISBN 979-8-4007-0108-5/23/10...\$15.00

<https://doi.org/10.1145/3581783.3612147>

KEYWORDS

Dynamic Vision Sensor (DVS); Spiking Neural Network (SNN); Deep Reinforcement Learning (DRL); dynamic obstacle avoidance.

ACM Reference Format:

Yang Wang, Bo Dong, Yuji Zhang, Yunduo Zhou, Haiyang Mei, Ziqi Wei, and Xin Yang. 2023. Event-Enhanced Multi-Modal Spiking Neural Network for Dynamic Obstacle Avoidance. In *Proceedings of the 31st ACM International Conference on Multimedia (MM '23)*, October 29–November 3, 2023, Ottawa, ON, Canada. ACM, New York, NY, USA, 11 pages. <https://doi.org/10.1145/3581783.3612147>

1 INTRODUCTION

In robotics, obstacle avoidance is a fundamental yet challenging task of satisfying the control objective subject to non-intersection or non-collision position constraints. Autonomous obstacle avoidance is of vital importance for an intelligent agent such as a mobile robot to navigate in its environment and attracts more and more research attention in recent years [28, 30, 54, 55] due to the growing need of practical usages such as post-disaster rescue [40] and subterranean detection [15]. In order to be able to perform tasks in some high-risk or inaccessible scenarios instead of humans, the mobile robot needs to possess strong capabilities of robust and efficient autonomous navigation and dynamic obstacle avoidance.

A dependable autonomous navigation and obstacle avoidance algorithm, unlike the path planning method which involves the pre-computation of an obstacle-free path, needs to be implemented as a *reactive* control law and should be *energy-efficient* due to the limited computational resources on the mobile robots. As to the former, deep reinforcement learning (DRL) techniques [27] are widely used to train an agent to make good obstacle avoidance decisions in complex/unknown environments [46]. As to the latter, the biologically realistic spiking neural network (SNN) [4] in which neurons compute asynchronously and communicate through spikes is leveraged by existing state-of-the-art methods to achieve low

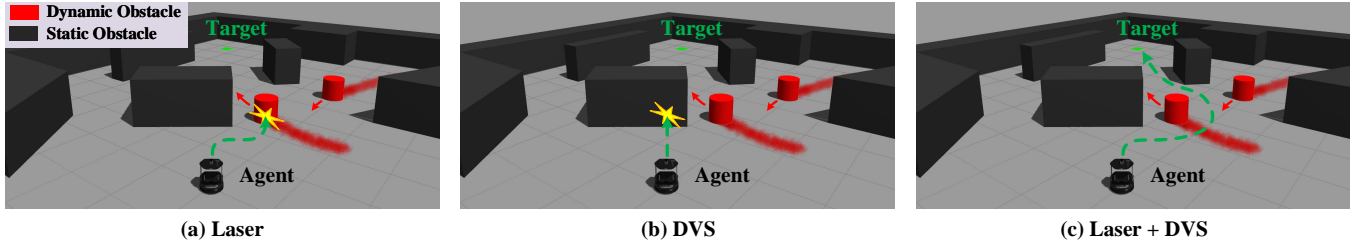


Figure 1: Illustration of obstacle avoidance using different sensors: (a) Laser can help detect large static objects but fails to perceive fast-moving objects; (b) event camera DVS excels to capture moving objects but cannot provide depth information to avoid large textureless obstacles; and (c) combining Laser and DVS achieves robust obstacle avoidance.

power consumption and low latency obstacle avoidance [1, 6, 43]. With recent advances in deep learning, training SNN with RL for obstacle avoidance becomes the mainstream method in the field and achieves promising results. However, existing methods typically assume that the environment is static [2, 33] while in real-world scenes such as malls and streets, the obstacles (e.g., pedestrians and vehicles) are not always static but often *dynamic*. The movement of obstacles makes the scene become more complex and leads to a faster relative speed between the agent and the obstacle, which requires the agent to make decisions and take avoidance actions in a shorter time, posing a great challenge to the existing methods.

In this work, we strive to embrace challenges toward robust *dynamic obstacle avoidance*. We approach this twofold. First, based on that the neuromorphic event camera called Dynamic Vision Sensor (DVS) [10, 20] can record a *high-frequency* stream of asynchronous brightness change events with extremely *low latency* (in the order of μs) and *low power consumption*, we for the first time introduce the two-dimensional DVS event modality into the SNN-based obstacle avoidance framework to provide motion cues complementary to the traditional Laser depth data for handling dynamic obstacles, building an omni perception of scenes, similar to human stereo vision [24]. Second, we develop an event-enhanced multimodal spiking actor network (EEM-SAN) that achieves dynamic obstacle avoidance in a deep reinforcement learning manner. EEM-SAN is built on three key modules: (i) a hybrid spiking variational autoencoder (HSVAE) that extracts information from DVS event data via unsupervised representation learning; (ii) a population coding (PC) module that combines population coding [44] and Poisson coding [43] to decode information from the activity of neurons; and (iii) a middle fuse decision module with learnable thresholding (MFDMLT) designed for multimodal data fusion.

We perform extensive experiments to demonstrate the efficacy of our method and show that DVS events provide a powerful and complementary cue for dynamic obstacle avoidance (Figure 1). In summary, our contributions are:

- the first solution to solve the challenging dynamic obstacle avoidance problem using a deep-reinforcement-learning-based spiking neural network with robot state and both Laser and DVS data as input, action decision as output;
- a novel hybrid spiking variational autoencoder that decouples the representation learning of DVS event data from the whole reinforcement learning and greatly facilitates the training process;

- a new middle fuse decision module with learnable thresholding to robustly integrate Laser and DVS data.

2 BACKGROUND AND RELATED WORK

Leaky Integrate-and-Fire (LIF) spiking neuron model. A spiking neural network (SNN) is a bio-plausible neural network that simulates biological information processing: neurons exchange information through spikes (or action potentials). Many different mathematical spiking neuron models have been developed, spanning from the simplest Integrate-and-Fire (IF) [32] to sophisticated Spike Response Model (SRM) [11]. Our approach leverages the *Leaky Integrated-and-Fire (LIF) model* [12], a simplified variant of SRM model. We can define an n_l -layer feedforward SNN architecture with LIF neurons. Given N^l incoming spike trains at layer l , $s_i^l(t)$, the SNN forward propagation is mathematically defined as:

$$\begin{aligned}
 v_i^{l+1}(t) &= \sum_{j=1}^{N^l} w_{ij} s_j^l(t) + \\
 &v_i^{l+1}(t-1) f_d \left(s_i^{l+1}(t-1) \right) + b_i^{l+1}, \\
 s_i^{l+1}(t) &= f_s \left(v_i^{l+1}(t) \right), \\
 f_d(s(t)) &= \begin{cases} D & s(t) = 0 \\ 0 & s(t) = 1 \end{cases}, \quad (1)
 \end{aligned}$$

where w_{ij} is the synaptic weight between the j -th neuron on the l -th layer and the i -th neuron on the layer $l+1$; b_i^{l+1} is an adjustable bias, and D is a constant. The operator $f_s(\cdot)$ is a spike function defined as:

$$f_s(v) : v \rightarrow s, s(t) := s(t) + \delta(t - t^{(f+1)}), \quad (2)$$

$$t^{f+1} = \min\{t : v(t) = \Theta, t > t^{(f)}\}, \quad (3)$$

where $s(t)$ is a sequence of spikes called a spike train, δ is a mathematical function whose value is zero everywhere except at zero and whose integral over the entire real line is equal to one, and Θ is the membrane potential threshold which is static and the same for all neurons in the network [41].

Dynamic Vision Sensor. DVS is a bio-inspired sensor that reports per-pixel brightness changes in log scale as a stream of asynchronous events [10, 25]. Compared to conventional frame-based cameras, DVS offers a very high dynamic range (140 dB versus 60 dB)

and high temporal resolution (in the order of μs). An event, e , encodes three pieces of information: the pixel location, (x, y) , of an event, the timestamp, t , records the time when the event is triggered, and the polarity, $p \in \{-1, 1\}$, of an event, which reflects the direction of the changes. Formally, a set of events can be defined as

$$\mathcal{E} = \{e_k\}_{k=1}^N = \{[x_k, y_k, t_k, p_k]\}_{k=1}^N. \quad (4)$$

In constant lighting conditions, events are triggered by moving edges (e.g., object contour and texture boundaries), making the DVS a natural edge extractor. However, this attractive feature also poses a unique challenge since events predominantly stem from edges, making the measured events inherently sparse. Asynchronous and sparse events cannot be effectively handled by CNN-based approaches designed for conventional frames.

DVS-based Robot Control. Most robotics applications use traditional frame-based cameras as their perception devices. However, frame-based cameras have inherent characteristics such as high data volume, low temporal resolution, and high latency, which weakens their ability to perceive fast-moving objects and greatly limit the robot’s manipulation capabilities. In this context, event cameras have attracted the attention of scholars in the field of robotics. By combining event cameras with robot perception and control, a series of breakthroughs in robot control has emerged, overcoming the limitations of traditional frame-based cameras. [29] is the first work to use DVS to avoid high-speed moving objects. To further explore the advantages of DVS, Falanga *et al.*[8] conducted experiments on UAVs equipped with three sensors: monocular, stereo frame-based cameras, and DVS. The results showed that the DVS ($2 \sim 4 ms$) had significantly lower delay than the monocular ($26 \sim 40 ms$) and stereo frame-based cameras ($17 \sim 70 ms$) when operating within the perception range of $2 m$. Sanket *et al.*[34] used an artificial neural network (ANN) to segment independent moving objects from event streams, and reasoned about their 3D motion to perform evasion tasks. Most of these methods rely on hand-crafted features or priors (e.g., Kalman filter [29], optical flow [8], and the obstacles [34]) to perform obstacle reasoning and avoidance. Our method differs from the above works in that we combine DRL and SNN with DVS to achieve robot control, enabling continuous autonomous robot navigation and robust yet efficient dynamic obstacle avoidance.

SNNs for Multimodal-Based Sensing. SNNs have not been widely explored for multimodal-based sensing [52, 53]. A few attempts have been made to combine image and audio modality. Liu *et al.*[22] developed a weighted-sum-based attention scheme to fuse image and audio modalities. The weights for each modality are dynamically decided. In the same vein, Jia *et al.*[13] proposed an MR-SNN algorithm to fuse the same two modalities using a fusion mask. MR-SNN learns a Motif mask for each modality and generates a fusion mask by averaging the two learned masks. Instead of learning in a supervised manner, Rathi *et al.*[31] proposed an unsupervised multimodal learning method, which combines the image and audio modality by learning cross-modal connections enabled by the Spike Timing Dependent Plasticity (STDP) algorithm. All these methods assess their effectiveness with a simple MNIST classification task. We validate our multimodal-based SNN approach with a more complex practical problem (i.e., obstacle avoidance), under both static and dynamic conditions.

SNNs for Robot Control. SNNs get substantial attention from the robot control community due to their high energy efficiency when deployed on neuromorphic hardware. A thread of work leverages SNNs for robot obstacle avoidance tasks [23, 33, 43]. Tang *et al.*[43] proposed a hybrid framework SDDPG for mapless navigation tasks. The SDDPG framework consists of an SNN-based actor network and a CNN-based critic network, where the two networks are co-trained together. Ding *et al.*[7] proposed a bio-inspired dynamic spiking threshold scheme to enhance SDDPG’s homeostasis in obstacle avoidance tasks under normal and degraded conditions. Later, Tang *et al.*[44] extended their approach to continuous control tasks and proposed the PopSAN method. An essential contribution introduced by PopSAN is the population-coding scheme, which effectively addresses the high-dimensional state problem presented in continuous control tasks. Recently, Zhang *et al.*[51] combined multiscale dynamic neurons coding and population coding to improve the performance of a spiking actor network. A critical difference between our approach and these methods is that we leverage two modalities for robot control instead of one.

3 METHODOLOGY

Figure 2(a) illustrates the diagram of our proposed event-enhanced multimodal spiking actor network (EEM-SAN) that is trained with reinforcement learning. First, the DVS sensor mounted on the agent records a high-frequency stream of brightness change events which is then encoded by a hybrid spiking variational autoencoder (HSVAE) (Figure 2(b)) into a one-dimensional vector (i.e., DVS State). Then, the obtained DVS state, together with the robot state and Laser state, is processed by a population coding (PC) module (Figure 2(c)) that can decode information from the activity of neurons. Finally, a middle fuse decision module with learnable thresholding (MFDM-LT) (Figure 2(d)) is used to fuse multimodal data and output obstacle avoidance decision which will be decoded into actual control action by Algorithm 1.

3.1 Hybrid Spiking Variational Autoencoder

To exploit useful motion cues embedded in DVS event data, a key problem is how to effectively and efficiently learn its feature representations. Variational Autoencoder (VAE) [18] is a powerful tool to extract the high-level embeddings of the input data. It typically consists of an encoder and decoder networks and is trained by:

$$Loss = \frac{1}{w \times h} \sum_{i,j} (x_{i,j} - \bar{x}_{i,j})^2 + \int p(x) \log \frac{p(x)}{q(x)}, \quad (5)$$

where the first item is the mean squared error (MSE) between the original input image x and the reconstruction \bar{x} , and the second item measures how the latent vector $p(x)$ matches a unit Gaussian $q(x)$ by Kullback-Leibler (KL) divergence. w and h represent the width and height of the event frame, respectively. VAEs have stable learning abilities in generative models and can be applied to various tasks. Recently, a series of works have attempted to use SNNs to create VAEs and make validation on classification datasets [36, 38, 42]. To take full advantage of the event-based nature of the continuous DVS stream and its rich temporal features, we design a novel hybrid spiking variational autoencoder (HSVAE) that contains

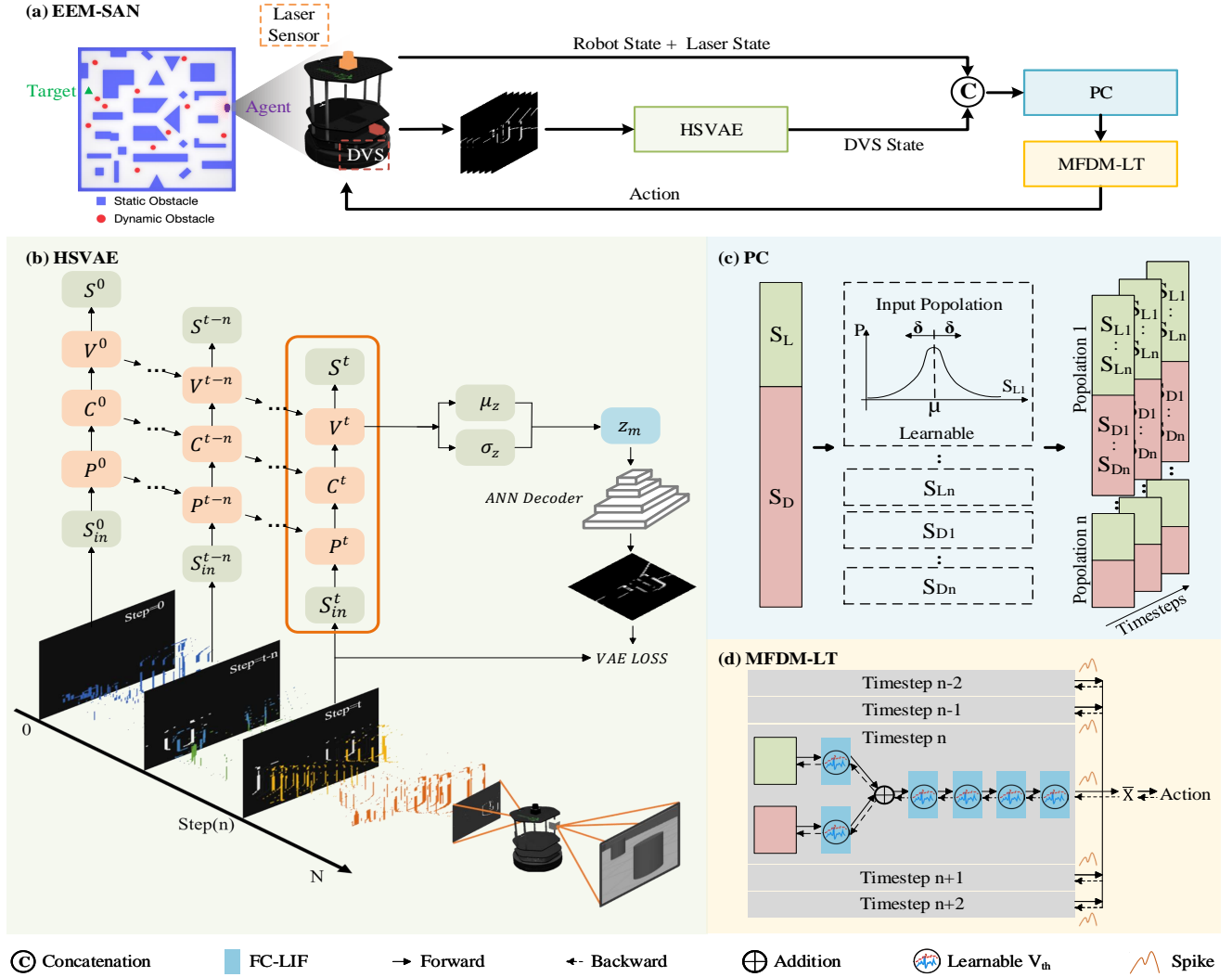


Figure 2: Overview of EEM-SAN (a) and its three main components: (b) a Hybrid Spiking Variational Autoencoder (HSVAE) module, (c) a Population Coding (PC) module, and (d) a Middle Fuse Decision Module with Learnable Thresholding (MFDM-LT).

an SNN encoder and ANN decoder. The architecture details of HSVAE are shown in Table 1. Unlike traditional spiking neural networks that reset the membrane potential, our method records all SNN-related states during one episode of simulated environment interaction. We record the current value, membrane potential and spike value of every neuron during one episode for the complete backpropagation chain. During deployment, we only need to record the relevant states at the last moment. We verified that SNNs trained in this way can integrate more temporal information to make better decisions. A single SNN layer of our HSVAE is shown in Figure 2(b) where refractory states are omitted for clarity. As illustrated, a stream of events recorded by the event camera mounted on a mobile robot is fed into SNN that can encode the spatio-temporal features of the input data into a latent state z . In Figure 2(b), P is pre-synaptic potential, C is current value and V is the membrane potential of the spiking neuron. The training process of HSVAE is presented in Algorithm 2.

Table 1: Architecture of our Hybrid Spiking VAE (HSVAE).

Layer	Kernel	Output	Layer Type
input		128×128×1	DVS128
1	16c4p1s2	64×64×16	SNN LIF Encoder
2	32c4p1s2	32×32×32	
3	16c4p1s2	16×16×16	
4	1c4p1s2	8×8×1	
5	-	64	Flatten()
6	-	64	$\mu = FC(V^t)$
7	-	64	$\sigma = FC(V^t)$
8	-	8×8×1	UnFlatten()
9	16c4p1s2	16×16×16	ANN Decoder
10	32c4p1s2	32×32×32	
11	16c4p1s2	64×64×16	
12	1c4p1s2	128×128×1	Event Frame

Notation: XcYpZsS represents channel X convolution filters (YxY) with padding Z and stride S.

Algorithm 1 Forward propagation through EEM-SAN

Ensure: Left and right wheel speeds v_L, v_R
Require: Min and max wheel speeds v_{min}, v_{max}
Require: Robot State, Laser State, Event frame Deque:
 $D_E = (E_1, \dots, E_5)$
Require: Learnable encoding means μ and standard deviations σ for all populations
Require: Middle Fuse Module: MF and total timestep T
DVS state generated by the Spiking Encoder of HSWAE: **DVS State** = HSWAE (D_E)
Input Multimodal Observation $O = [\text{Robot State}, \text{Laser State}, \text{DVS State}]$
Spikes generated by the population coding module:
 $\mathbf{X} = \text{PC}(\mathbf{o}, \mu, \sigma)$
for $t = 1, \dots, T$ **do**
 Laser spikes from populations at timestep t :
 $\mathbf{S}_L^{(t)(0)} = \mathbf{X}^{(t)(O_0 \dots O_L)}$
 DVS spikes from populations at timestep t :
 $\mathbf{S}_D^{(t)(0)} = \mathbf{X}^{(t)(O_D \dots O_{end})}$
 Fuse spikes from Middle Fuse Module:
 $\mathbf{S}_M^{(t)(0)} = MF(\mathbf{S}_L^{(t)(0)}, \mathbf{S}_D^{(t)(0)})$
 for $k = 1, \dots, K$ **do**
 Update LIF neurons in layer K at timestep t based on spikes from layer $k-1$:
 $\mathbf{c}^{(t)(k)} = d_c \cdot \mathbf{c}^{(t-1)(k)} + \mathbf{W}^{(k)} \mathbf{s}^{(t)(k-1)} + \mathbf{b}^{(k)}$;
 $\mathbf{v}^{(t)(k)} = d_v \cdot \mathbf{v}^{(t-1)(k)} \cdot (1 - \mathbf{s}^{(t-1)(k)}) + \mathbf{c}^{(t)(k)}$;
 $\mathbf{s}^{(t)(k)} = \text{Threshold}(\mathbf{v}^{(t)(k)})$;
 end for
 $\text{SpikeCount}^t = \text{SpikeCount}^{t-1} + \mathbf{s}^{(t)(l)}$
end for
Action = $\text{SpikeCount}^{(T)} / T$
 $v_L = \text{Action}[0] * (v_{max} - v_{min}) + v_{min}$
 $v_R = \text{Action}[1] * (v_{max} - v_{min}) + v_{min}$

3.2 Population Coding

Neurons in the brain often use population coding and it isn't easy to decode correct information from the activity of a single neuron [39]. Hence, some researchers have begun to use populations of neurons to encode information into spike trains fed into SNNs instead of simple frequency encoding (e.g., Poisson coding) [44, 51]. To encode each dimension of the state, we created a population with 10 neurons, where each neuron has a Gaussian receptive field with two parameters: mean and standard deviation. These parameters were learned with surrogate backpropagation. Since SAN adopts the Poisson encoding, we apply the group encoding method combined with Poisson coding as PopSAN method in our experimental comparison. For a fair comparison, our method takes the same population and Poisson coding. Formally, the population coding function can be formulated as:

$$\begin{cases} A_{P_{i,j}} = \text{EXP}(-1/2 \cdot ((s_i - \mu_{i,j})/\sigma_{i,j})^2) \\ \mathbf{A}_P = [A_{P_{1,1}}, \dots, A_{P_{i,j}}, \dots, A_{P_{N,J}}] \end{cases}, \quad (6)$$

$$P(O_{k,t} = 1) = C_R^r A_{P_k}^r (1 - A_{P_k})^{R-r}, \quad (7)$$

Algorithm 2 Spiking Neural Network Encoder Training

Initialize the memory D to store event frame observations, set the episode number T , set $e_num = 0$;
Start the simulation environment;
while $e_num < T$ **do**
 Randomly set the start and goal locations in our training environment;
 while not collision do
 Capture the Event frame X_t , store X_t in D_T ;
 Move with the linear and angular velocity ;
 end while
end while
for $epoch = 1, T$ **do**
 Initialize the SNN state C_i, V_i, S_i in every layer;
 for $X_t = 1, D_t$ **do**
 Update θ_0 through on the loss defined in formula (4) and update SNN state C_i, V_i, S_i through STBP algorithm;
 end for
end for

where i is the index of the input state ($i = 1, \dots, N$), j is the index of neurons in a population ($j = 1, \dots, J$), and A_P is the stimulation strength after population coding, used for drawing the binary random number [51].

3.3 Middle Fuse Decision Module with Learnable Thresholding

The middle fuse decision module consists of a middle fuse (MF) module and a decision module (DM). In MF, two modalities are first transformed to a one-dimensional vector with a length of 20 by two fully connected layers composed of LIF neurons, respectively, and the two obtained one-dimensional vectors are then fused via the element-wise addition. DM contains four fully connected SNN layers and its forward propagation process is presented in Algorithm 1. Since the threshold function of SNNs is non-differentiable, many methods focus on how to learn and tune it [5, 37, 50]. Among them, the approximate backpropagation method is widely due to its efficiency and flexibility. Here, we adopt the STBP [47] algorithm which uses the rectangular function to approximate the gradient of a spike as follows:

$$z(V) = \begin{cases} 1 & \text{if } |V - V_{th}| < 0.5 \\ 0 & \text{otherwise} \end{cases}, \quad (8)$$

where z is the pseudo-gradient, V is membrane potential, and V_{th} is the threshold.

Several dynamic thresholding schemes have been developed in recent years to make neuronal thresholds learnable and varied throughout the network. However, most existing methods require strict prerequisites or are not based on the gradient descent method, which results in a higher computational load or makes it difficult to migrate to other SNNs [16, 26]. A few attempts have been made to integrate with the existing back-propagation-based training algorithms on classification tasks [45, 49]. Following the path, we further explore the performance of learnable thresholds under multimodal reinforcement learning tasks. We use the learnable thresholding

mechanism in our MFDN. This mechanism is endowed with parameter optimization capability through STBP. By doing so, all neurons have different thresholds in the same network. This means the neuron's response depends not only on its internal state but also on the threshold level. The key idea of the learnable thresholding is to find the comprehensive gradient of the loss function, and then the weight W and the neuron's threshold H are simultaneously updated until convergence. From Eq. 1 and 8, the threshold's partial derivatives of the loss function can be calculated as follows:

$$\frac{\partial L}{\partial H^n} = \sum_{t=1}^T \frac{\partial L}{\partial s^{t,n}} \frac{\partial s^{t,n}}{\partial H^n}. \quad (9)$$

To ensure that the threshold remains within the appropriate area, we create a new parameter r to define H using hyperbolic tangent relation, formulated as $H = \tanh(r)$. With this, Eq. 9 can be expressed as:

$$\begin{aligned} \frac{\partial L}{\partial r^n} &= \sum_{t=1}^T \frac{\partial L}{\partial s^{t,n}} \frac{\partial s^{t,n}}{\partial H^n} \frac{\partial H^n}{\partial r^n} \\ &= - \sum_{t=1}^T \frac{\partial L}{\partial s^{t,n}} f'(v^{t,n} - \tanh(r^n))(1 - \tanh^2(r^n)). \end{aligned} \quad (10)$$

Improved in this way, the threshold H of the neurons can be iteratively trained using the backpropagation method and will be in the range $(-1, 1)$. In this context, we apply the learnable thresholding scheme to MFDN and let neurons in the same layer share the same threshold to reduce learnable parameters.

4 EXPERIMENTS AND EVALUATION

We evaluate the obstacle avoidance capabilities of the proposed EEM-SAN using success rate (SR) as a metric. SR is the percentage of successful passes among 200 trials. A successful pass is a trial in which a robot can reach the destination without touching any static or dynamic obstacles within 1000 steps. Our evaluation baseline model and test environment are modified variants of the SAN [43] and its original simulated test environment, respectively.

4.1 Experimental Settings

Implementation Details. We integrated the EEM-SAN with the deep reinforcement learning algorithm DDPG [21]. We repeated each experiment three times to obtain the mean success rate. The frequency of the Laser sensor and DVS are set to 20 Hz and 100 Hz, respectively. The timestep of MFDN-LT is set as 5. The number of groups in the population coding is set as 10. The neuron current decay constant and the voltage decay constant are set as 0.5 and 0.75, respectively. During the training process, we set the batch size to 256 and the learning rate to 0.0001.

Simulator Setup. Our experiments are based on the Gazebo simulator [19]. Both the training and testing use the robot operating system (ROS) as a middleware. The testing environment was set to be different from the training environment for better validating the generalization capability of a method. Following existing methods SAN [43], PopSAN [44], and BDETT [7], we developed and tested our method in the same environment and with the same random seeds. Our testing environments are set to be very challenging to

better validate the robustness of an obstacle avoidance method. The challenges of our testing environments are in the following aspects: (i) **densely and highly dynamic obstacles** (eleven dynamic obstacles, all set to higher than the maximum speed of the robot); (ii) **faster robot speed** (the maximum speed of the robot is twice that in SAN); and (iii) **narrower traversal passages and more densely organized static obstacles**. We have experimentally demonstrated in Table 2 that the existing SOTA method SAN [43] has a significant accuracy drop (*i.e.*, from 97.8% to 58.0%) when transferred from common scenes to our challenging scenes. More details about training and testing environment can be found in Appendix and SAN [43].

4.2 Evaluation

We extensively compare the effectiveness of our proposed EEM-SAN to three state-of-the-art methods including SAN [43], PopSAN [44], and BDETT [7] across two different test maps [7, 43] under both dynamic and static conditions. The experimental results are reported in Table 2 and Figure 3.

Dynamic Conditions. To ensure the diversity and challenge of the scene, we set up eleven dynamic obstacles that reciprocate linearly along different trajectories at different speeds, and the speed of all moving obstacles is set to slightly higher than the maximum speed of the robot. From the results in Table 2, we can see that our EEM-SAN outperforms all competing methods by a significant margin. For example, compared with the state-of-the-art method BDETT [7], our method improves SR by 10.8% and 11.8% on the two testing maps, respectively. This clearly demonstrates the effectiveness of our method for dynamic obstacle avoidance.

Static Conditions. Although our method was originally designed for dynamic obstacle avoidance, we also tested its performance in static conditions to see its robustness. From Table 2, we observe that: (1) our method still performs the best among all the compared methods for static obstacle avoidance; (2) when varying the maximum robot speed from 1.0 m/s to 0.5 m/s, all the methods get significant performance improvement. This is because a robot with a slow-moving speed has more time to make a decision and take action, which greatly decreases the difficulty of obstacle avoidance. Under such a condition, our method achieves very robust avoidance, *i.e.*, the success rate SR is up to 1.000; (3) compared to SAN [43], the PopSAN [44] which is based on SAN [43] but equipped with population coding method instead of frequency coding performs better, especially for the robot with a maximum speed of 1.0 m/s. This indicates that the population coding method is more suitable for handling rapidly changing scenes than the frequency coding method; and (4) by comparing the results of BDETT [7] and PopSAN [44], the obvious performance improvement can be found under dynamic conditions but not under static conditions. This reveals that the dynamic thresholding scheme developed in BDETT [7] benefits much from the dynamic scenes but little from static conditions. By contrast, our method can significantly improve obstacle avoidance performance in both dynamic and static conditions. Furthermore, Figure 3 visualizes an example that clearly shows that the existing methods often fail around the right-angle turn while our method can achieve robust obstacle avoidance.

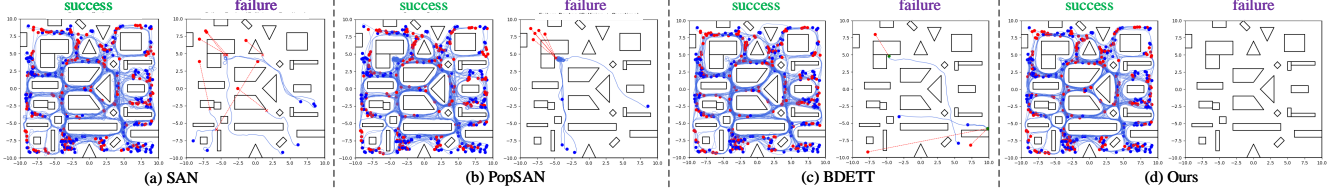


Figure 3: Success and failure trajectories of the four methods at the same 200 randomly sampled start and goal locations. The blue dot represents the starting point, the red dot represents the target point, and the green dot represents the overtime case.

Table 2: Quantitative performance of obstacle avoidance in both dynamic and static conditions on two different maps.

Methods	Dynamic Conditions		Static Conditions	
	Max Robot Speed	Max Robot Speed	Max Robot Speed	Max Robot Speed
	1.0 m/s	1.0 m/s	1.0 m/s	0.5 m/s
	Map 1 SR \uparrow / Map 2 SR \uparrow	Map 1 SR \uparrow / Map 2 SR \uparrow	Map 1 SR \uparrow / Map 2 SR \uparrow	Map 1 SR \uparrow / Map 2 SR \uparrow
SAN	0.580 / 0.577	0.645 / 0.560	0.978 / 0.966	
PopSAN	0.598 / 0.618	0.805 / 0.718	0.983 / 0.973	
BDETT	0.657 / 0.625	0.735 / 0.728	0.975 / 0.923	
Ours	0.765 / 0.743	0.870 / 0.848	1.000 / 0.985	

Table 3: Quantitative ablation results indicate that each component in EEM-SAN contributes to the overall performance.

	Laser Only	Laser + DVS Event			SR \uparrow
	PopSAN	E2E	HSVAE	MFDM-LT	
(a)	✓				0.598
(b)	✓	✓			0.705
(c)	✓		✓		0.728
(d)	✓		✓	✓	0.765

4.3 Ablation Study

To analyze our EEM-SAN, we investigate (a) the importance of DVS event cues; (b) the effectiveness of HSVAE; (c) the effectiveness of MFDM-LT; and (d) the efficiency advantage of SNN over ANN. Table 3, 4, 5, and Figure 4, 5 summarize our findings.

Importance of DVS Event Cues. We conduct an experiment to better understand the benefit of including DVS event cues for dynamic obstacle avoidance. Based on the baseline method PopSAN [44] (Table 3 (a)), we introduce the DVS event modality and implement an end-to-end (E2E) framework with naive modality fusion (*i.e.*, addition). The SR of (b) is much higher (*i.e.*, 10.7%) than that of (a), indicating DVS event is a strong cue for robust dynamic obstacle avoidance.

Effectiveness of HSVAE. Based on “E2E” (Table 3 (b)), adopting our proposed HSVAE (Table 3 (c)) improves the SR from 0.705 to 0.728. This demonstrates that our HSVAE can better extract information from DVS events frame for the decision making in obstacle avoidance. Furthermore, our HSVAE can be trained independently in advance and can be embedded in EEM-SAN with fixed weights during the reinforcement learning process. Without the need of saving/updating intermediate states like the DVS information extraction encoder in “E2E”, our HSVAE can help save lots of GPU

Table 4: Performance comparison between different DVS information encoding methods.

Methods	AVAE	FSVAE	HSVAE (ours)
SR \uparrow	0.677	0.673	0.728

Table 5: Comparison of the average amount of computation required to infer single state to action during one episode.

	Architecture		Computational Complexity	
	HSVAE	MFDM-LT	Addition	Multiplication
(i)	SNN	SNN	1.33×10^7	0.52×10^7
(ii)	ANN	SNN	5.87×10^7	5.78×10^7
(iii)	SNN	ANN	1.63×10^7	0.85×10^7
(iv)	ANN	ANN	6.16×10^7	6.11×10^7

memory consumption and speed up the reinforcement learning process. Our HSVAE consists of an SNN encoder equipped with temporal information integration and an ANN decoder. It accommodates SNNs and ANNs in different layers, enabling the benefits of SNNs for sparse event data processing and ANNs for maintaining performance. The reason for using a hybrid architecture is that the spike activities decrease significantly as the network depth increases and the ANN decoder does not need to run during deployment. The experimental results in Table 4 show that our HSVAE performs better than its ANN counterpart (AVAE) and the Fully Spiking Variational Autoencoder (FSVAE) [14] whose encoder can not integrate temporal spikes information. This demonstrates that (i) the SNN encoder is more suitable for DVS information extraction than the ANN encoder; (ii) the temporal information integration is needed in the SNN encoder for the continuous obstacle avoidance decision; and (iii) the ANN decoder yields better results than the SNN decoder.

Effectiveness of MFDM-LT. Based on Table 3 (c), replacing the naive addition modality fusion with our designed MFDM-LT (Table 3 (d)) can greatly enhance the performance. To explore how the MFDM-LT works, we visualize the learned threshold values of different layers in the MFDM-LT module under different initial training threshold settings in Figure 4. We can see that the learned thresholds of Laser and DVS layers are not equal. This shows that the Laser and DVS modalities contribute differently to the obstacle avoidance action. Besides, the learned threshold of DVS layer is higher than that of Laser layer for all the initial training threshold

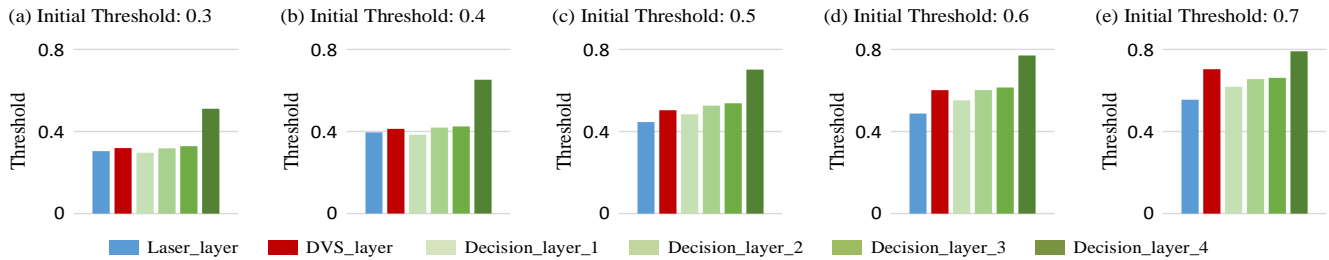


Figure 4: Comparison between learned thresholds in different MFDM-LT layers under different initial training thresholds.

settings. The reason behind this may be (i) the DVS modality generates larger amount of data and thus a higher threshold is needed to filter out the useless spikes and (ii) lower threshold in Laser layer enables more depth information to pass through to dominate the action decision at the startup phase of the robot when lots of DVS events noise would be generated to interfere with decision making. Another interesting finding is that the threshold values in the decision layers increase as the network goes deeper. This phenomenon can be explained as the modality-fused data can fire neurons in shallow layers easily to maintain sufficient information which would be filtered by deep-layer neurons strictly to extract most informative data for the final action decision. Furthermore, we fix the learnable thresholds in MFDM-LT during the training process (Figure 5 MFDM) and find that the performance degrades dramatically. And this can be a strong evidence to demonstrate the effectiveness of the learnable threshold scheme in our MFDM-LT.

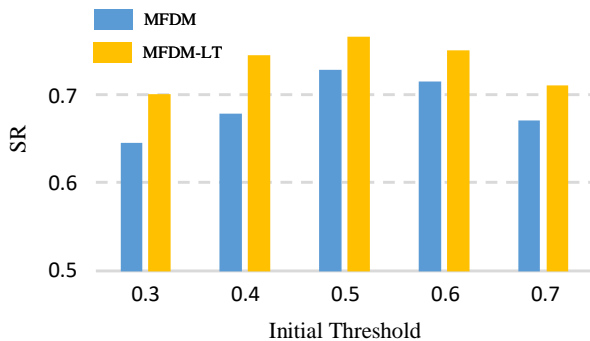


Figure 5: Performance comparison between MFDM variants with and without learnable threshold scheme under different initial training thresholds settings.

Efficiency Advantage of SNN over ANN. Both HSVAE and MFDM-LT modules in our EEM-SAN are implemented by SNN, but not ANN. To show the advantage of such a choice, we compare the superior computational efficiency of our fully-SNN-based EEM-SAN against its ANN variants in terms of addition and multiplication FLOPs in Table 5. We can observe that, compared with the fully-SNN-based architecture (Table 5 (i)), much more computations are required when adopting ANN-based HSVAE (ii), ANN-based MFDM-LT (iii), or fully-ANN-based network (iv). For example, the ANN version of EEM-SAN (iv) is 4.63 and 11.66 times more expensive than the SNN version (i) in terms of addition and multiplication operations, respectively. Prior works [14, 17, 48] have

demonstrated that the computing complexity of the network is positively correlated with inference speed and energy consumption, especially when the network is implemented in neuromorphic device [3, 35, 43]. Therefore, our fully-SNN-based EEM-SAN can achieve much faster inference with much lower energy consumption than its ANN counterpart.

4.4 Limitations

In this work, we make the first attempt to connect multi-sensor representation and fully-SNN-based DRL towards robust and efficient robot control in extreme navigation scenarios with both static and fast-moving dynamic obstacles. Testing our method on different robot platforms (e.g., unmanned aerial vehicles) with more real challenging scenes (e.g., subterranean) would be a promising future work but out of focus of this work. Besides, our EEM-SAN has only been tested in a realistic simulator and has not been implemented on a real robot due to the unavailability of neuromorphic hardware. To conduct such an engineering verification, we are actively seeking permission from the Intel Neuromorphic Research Community (INRC) to use the neuromorphic chip Loihi. We will perform such an interesting verification once the hardware becomes available.

5 CONCLUSION

In this paper, we presented an event-enhanced multimodal spiking actor network (EEM-SAN) for autonomous navigation and dependable obstacle avoidance. Our solution is the first to introduce the Dynamic Vision Sensor (DVS) to provide motion cues that complement the traditional Laser depth data for handling dynamic obstacles. EEM-SAN consists of two main modules: a hybrid spiking variational autoencoder (HSVAE) which encodes the DVS event data through unsupervised representation learning, and a middle fuse decision module with learnable thresholding (MFDM-LT) designed for multimodal data fusion. Through extensive validation and ablation studies, we demonstrate the value of DVS event cues, as well as the effectiveness and robustness of our EEM-SAN. In the future, we plan to deploy our method on neuromorphic devices to maximize its advantages in terms of computational efficiency and energy consumption.

ACKNOWLEDGMENTS

This work was supported in part by National Key Research and Development Program of China (2022ZD0210500), the National Natural Science Foundation of China under Grants 61972067/U21A20491, and the Distinguished Young Scholars Funding of Dalian (No. 2022RJ01). Ziqi Wei was supported by the open funding of State Key Laboratory of Structural Analysis for Industrial Equipment.

REFERENCES

- [1] Ignacio Abadía, Francisco Naveros, Eduardo Ros, Richard R Carrillo, and Niceto R Luque. 2021. A cerebellar-based solution to the nondeterministic time delay problem in robotic control. *Science Robotics* 6, 58 (2021), eabf2756.
- [2] Riku Arakawa and Shintaro Shiba. 2020. Exploration of reinforcement learning for event camera using car-like robots. *arXiv preprint arXiv:2004.00801* (2020).
- [3] Hermann Blum, Alexander Dietmüller, Moritz Milde, Jörg Conradt, Giacomo Indiveri, and Yulia Sandamirskaya. 2017. A neuromorphic controller for a robotic vehicle equipped with a dynamic vision sensor. *Robotics Science and Systems, RSS 2017* (2017).
- [4] Sander M Bohte, Joost N Kok, and Han La Poutre. 2002. Error-backpropagation in temporally encoded networks of spiking neurons. *Neurocomputing* (2002).
- [5] Xiang Cheng, Tielin Zhang, Shuncheng Jia, and Bo Xu. 2020. Finite meta-dynamic neurons in spiking neural networks for spatio-temporal learning. *arXiv preprint arXiv:2010.03140* (2020).
- [6] Travis DeWolf. 2021. Spiking neural networks take control. *Science Robotics* 6, 58 (2021), eabk3268.
- [7] Jianchuan Ding, Bo Dong, Felix Heide, Yufei Ding, Yunduo Zhou, Baocai Yin, and Xin Yang. 2022. Biologically Inspired Dynamic Thresholds for Spiking Neural Networks. In *Advances in Neural Information Processing Systems*.
- [8] Davide Falanga, Suseong Kim, and Davide Scaramuzza. 2019. How fast is too fast? the role of perception latency in high-speed sense and avoid. *IEEE Robotics and Automation Letters* 4, 2 (2019), 1884–1891.
- [9] C. Florensa, D. Held, M. Wulfmeier, and P. Abbeel. 2017. Reverse Curriculum Generation for Reinforcement Learning. (2017).
- [10] Guillermo Gallego, Tobi Delbrück, Garrick Orchard, Chiara Bartolozzi, Brian Taba, Andrea Censi, Stefan Leutenegger, Andrew J Davison, Jörg Conradt, Kostas Daniilidis, et al. 2020. Event-based vision: A survey. *IEEE transactions on pattern analysis and machine intelligence* (2020).
- [11] Wulfram Gerstner. 1995. Time structure of the activity in neural network models. *Physical review E* (1995).
- [12] Wulfram Gerstner and Werner M Kistler. 2002. *Spiking neuron models: Single neurons, populations, plasticity*. Cambridge university press.
- [13] Shuncheng Jia, Ruichen Zuo, Tielin Zhang, Hongxing Liu, and Bo Xu. 2022. Motif-Topology and Reward-Learning Improved Spiking Neural Network for Efficient Multi-Sensory Integration. In *IEEE International Conference on Acoustics, Speech and Signal Processing (ICASSP)*. 8917–8921.
- [14] Hiromichi Kamata, Yusuke Mukuta, and Tatsuya Harada. 2022. Fully spiking variational autoencoder. In *Proceedings of the AAAI Conference on Artificial Intelligence*.
- [15] S. Khattak, H. D. Nguyen, F. Mascarich, T. Dang, and K. Alexis. 2020. Complementary Multi-Modal Sensor Fusion for Resilient Robot Pose Estimation in Subterranean Environments. In *IEEE International Conference on Unmanned Aircraft Systems 2020*.
- [16] Taeyoon Kim, Suman Hu, Jaewook Kim, Joon Young Kwak, Jongkil Park, Suyoun Lee, Inho Kim, Jong-Keuk Park, and YeonJoo Jeong. 2021. Spiking neural network (snn) with memristor synapses having non-linear weight update. *Frontiers in computational neuroscience* 15 (2021), 646125.
- [17] Youngeun Kim, Hyoungseob Park, Abhishek Moitra, Abhiroop Bhattacharjee, Yeshwanth Venkatesha, and Priyadarshini Panda. 2022. Rate Coding Or Direct Coding: Which One Is Better For Accurate, Robust, And Energy-Efficient Spiking Neural Networks?. In *IEEE International Conference on Acoustics, Speech and Signal Processing (ICASSP)*. 71–75.
- [18] Diederik P Kingma and Max Welling. 2013. Auto-encoding variational bayes. *arXiv preprint arXiv:1312.6114* (2013).
- [19] Nathan Koenig and Andrew Howard. 2004. Design and use paradigms for gazebo, an open-source multi-robot simulator. In *2004 IEEE/RSJ International Conference on Intelligent Robots and Systems (IROS)*(IEEE Cat. No. 04CH37566). Vol. 3. IEEE, 2149–2154.
- [20] P. Lichtsteiner, C. Posch, and T. Delbruck. 2008. A $128 \times 128 \times 120$ dB $15 \mu\text{s}$ Latency Asynchronous Temporal Contrast Vision Sensor. *IEEE Journal of Solid-State Circuits* 43, 2 (2008), 566–576.
- [21] Timothy P Lillicrap, Jonathan J Hunt, Alexander Pritzel, Nicolas Heess, Tom Erez, Yuval Tassa, David Silver, and Daan Wierstra. 2015. Continuous control with deep reinforcement learning. *arXiv preprint arXiv:1509.02971* (2015).
- [22] Qianhui Liu, Dong Xing, Lang Feng, Huajin Tang, and Gang Pan. 2022. Event-Based Multimodal Spiking Neural Network with Attention Mechanism. In *IEEE International Conference on Acoustics, Speech and Signal Processing (ICASSP)*. 8922–8926.
- [23] Amarnath Mahadevuni and Peng Li. 2017. Navigating mobile robots to target in near shortest time using reinforcement learning with spiking neural networks. In *International Joint Conference on Neural Networks (IJCNN)*. 2243–2250.
- [24] David Marr and Tomaso Poggio. 1979. A computational theory of human stereo vision. *Proceedings of the Royal Society of London. Series B. Biological Sciences* 204, 1156 (1979), 301–328.
- [25] Haiyang Mei, Zuowen Wang, Xin Yang, Xiaopeng Wei, and Tobi Delbruck. 2023. Deep polarization reconstruction with PDAVIS events. In *Proceedings of the IEEE/CVF Conference on Computer Vision and Pattern Recognition*.
- [26] Qingyan Meng, Mingqing Xiao, Shen Yan, Yisen Wang, Zhouchen Lin, and Zhi-Quan Luo. 2022. Training High-Performance Low-Latency Spiking Neural Networks by Differentiation on Spike Representation. In *Proceedings of the IEEE/CVF Conference on Computer Vision and Pattern Recognition*. 12444–12453.
- [27] Volodymyr Mnih, Koray Kavukcuoglu, David Silver, Andrei A Rusu, Joel Veness, Marc G Bellemare, Alex Graves, Martin Riedmiller, Andreas K Fidjeland, Georg Ostrovski, et al. 2015. Human-level control through deep reinforcement learning. *nature* 518, 7540 (2015), 529–533.
- [28] Michael Montemerlo, Sebastian Thrun, Daphne Koller, Ben Wegbreit, et al. 2002. FastSLAM: A factored solution to the simultaneous localization and mapping problem. *Aaai/iaai* 593598 (2002).
- [29] Elias Mueggler, Nathan Baumli, Flavio Fontana, and Davide Scaramuzza. 2015. Towards evasive maneuvers with quadrotors using dynamic vision sensors. In *2015 European Conference on Mobile Robots (ECMR)*. IEEE, 1–8.
- [30] Mark Pfeiffer, Samarth Shukla, Matteo Turchetta, Cesar Cadena, Andreas Krause, Roland Siegwart, and Juan Nieto. 2018. Reinforced imitation: Sample efficient deep reinforcement learning for mapless navigation by leveraging prior demonstrations. *IEEE Robotics and Automation Letters* 3, 4 (2018), 4423–4430.
- [31] Nitin Rathi and Kaushik Roy. 2018. STDP based unsupervised multimodal learning with cross-modal processing in spiking neural networks. *IEEE Transactions on Emerging Topics in Computational Intelligence* 5, 1 (2018), 143–153.
- [32] Nitin Rathi and Kaushik Roy. 2020. Diet-snn: Direct input encoding with leakage and threshold optimization in deep spiking neural networks. *arXiv preprint arXiv:2008.03658* (2020).
- [33] Nikolaus Salvatore, Sami Mian, Collin Abidi, and Alan George. 2020. A Neuro-inspired Approach to Intelligent Collision Avoidance and Navigation. In *IEEE/AIAA 39th Digital Avionics Systems Conference*.
- [34] Nitin J Sanket, Chethan M Parameshwara, Chahat Deep Singh, Ashwin V Kurutukulam, Cornelia Fermüller, Davide Scaramuzza, and Yiannis Aloimonos. 2020. Evidodgenet: Deep dynamic obstacle dodging with event cameras. In *2020 IEEE International Conference on Robotics and Automation (ICRA)*. IEEE, 10651–10657.
- [35] Thorben Schoepe, Ella Janotte, Moritz B Milde, Olivier JN Bertrand, Martin Egelhaaf, and Elisabetta Chicca. 2021. Finding the gap: neuromorphic motion vision in cluttered environments. *arXiv preprint arXiv:2102.08417* (2021).
- [36] Nicolas Skatchkovsky, Osvaldo Simeone, and Hyeryung Jang. 2021. Learning to time-decode in spiking neural networks through the information bottleneck. *arXiv preprint arXiv:2106.01177* (2021).
- [37] Ioana Sporea and André Grünig. 2013. Supervised learning in multilayer spiking neural networks. *Neural computation* 25, 2 (2013), 473–509.
- [38] Kenneth Stewart, Andreea Danielescu, Lazar Supic, Timothy Shea, and Emre Neftci. 2021. Gesture similarity analysis on event data using a hybrid guided variational auto encoder. *arXiv preprint arXiv:2104.00165* (2021).
- [39] Wensheng Sun and Dennis L Barbour. 2017. Rate, not selectivity, determines neuronal population coding accuracy in auditory cortex. *PLoS biology* 15, 11 (2017), e2002459.
- [40] T. Takahashi, I. Takeuchi, T. Koto, S. Tadokoro, and I. Noda. 2000. RoboCup-Rescue Disaster Simulator Architecture. In *Robot Soccer World Cup*.
- [41] Doron Tal and Eric L Schwartz. 1997. Computing with the leaky integrate-and-fire neuron: logarithmic computation and multiplication. *Neural computation* 9, 2 (1997), 305–318.
- [42] Sameerah Talafha, Banafsheh Rekabdar, Christos Mousas, and Chinwe Ekenna. 2020. Biologically inspired sleep algorithm for variational auto-encoders. In *International Symposium on Visual Computing*. Springer, 54–67.
- [43] Guangzhi Tang, Neelesh Kumar, and Konstantinos P Michmizos. 2020. Reinforcement co-learning of deep and spiking neural networks for energy-efficient navigation with neuromorphic hardware. In *IEEE/RSJ International Conference on Intelligent Robots and Systems (IROS)*. 6090–6097.
- [44] Guangzhi Tang, Neelesh Kumar, Raymond Yoo, and Konstantinos P. Michmizos. 2020. Deep Reinforcement Learning with Population-Coded Spiking Neural Network for Continuous Control. In *Conference on Robot Learning*.
- [45] Siqi Wang, Tee Hiang Cheng, and Meng-Hiot Lim. 2022. LTMD: Learning Improvement of Spiking Neural Networks with Learnable Thresholding Neurons and Moderate Dropout. In *Advances in Neural Information Processing Systems*.
- [46] Yuanda Wang, Haibo He, and Changyin Sun. 2018. Learning to navigate through complex dynamic environment with modular deep reinforcement learning. *IEEE Transactions on Games* 10, 4 (2018), 400–412.
- [47] Yujie Wu, Lei Deng, Guoqi Li, Jun Zhu, and Luping Shi. 2018. Spatio-temporal backpropagation for training high-performance spiking neural networks. *Frontiers in neuroscience* 12 (2018), 331.
- [48] Man Yao, Guangshe Zhao, Hengyu Zhang, Yifan Hu, Lei Deng, Yonghong Tian, Bo Xu, and Guoqi Li. 2022. Attention spiking neural networks. *arXiv preprint arXiv:2209.13929* (2022).
- [49] Xingting Yao, Fanrong Li, Zitao Mo, and Jian Cheng. 2022. GLIF: A Unified Gated Leaky Integrate-and-Fire Neuron for Spiking Neural Networks. In *Advances in Neural Information Processing Systems*.
- [50] Yi Zeng, Tielin Zhang, and Bo Xu. 2017. Improving multi-layer spiking neural networks by incorporating brain-inspired rules. *Science China Information*

Sciences 60, 5 (2017), 1–11.

- [51] Duzhen Zhang, Tielin Zhang, Shuncheng Jia, and Bo Xu. 2022. Multiscale Dynamic Coding improved Spiking Actor Network for Reinforcement Learning. *AAAI (2022)*.
- [52] Haiwei Zhang, Jiqing Zhang, Bo Dong, Pieter Peers, Wenwei Wu, Xiaopeng Wei, Felix Heide, and Xin Yang. 2023. In the blink of an eye: Event-based emotion recognition. In *ACM SIGGRAPH 2023 Conference Proceedings*. 1–11.
- [53] Jiqing Zhang, Bo Dong, Haiwei Zhang, Jianchuan Ding, Felix Heide, Baocai Yin, and Xin Yang. 2022. Spiking Transformers for Event-Based Single Object Tracking. In *Proceedings of the IEEE/CVF Conference on Computer Vision and Pattern Recognition*.
- [54] Wenqi Zhang, Kai Zhao, Peng Li, Xiao Zhu, Yongliang Shen, Yanna Ma, Yingfeng Chen, and Weiming Lu. 2022. A Closed-Loop Perception, Decision-Making and Reasoning Mechanism for Human-Like Navigation. *arXiv preprint arXiv:2207.11901 (2022)*.
- [55] Wenqi Zhang, Kai Zhao, Peng Li, Xiao Zhu, Faping Ye, Weijie Jiang, Huiqiao Fu, and Tao Wang. 2021. Learning to Navigate in a VUCA Environment: Hierarchical Multi-expert Approach. In *IEEE/RSJ International Conference on Intelligent Robots and Systems*. 9254–9261.

In the appendix, we first present more evaluation results under both dynamic and static conditions in Section A, and then detail more experimental settings in Section B.

A MORE EVALUATION RESULTS

Figure 6 visualizes an example which clearly shows that the existing methods fail more times while our method can achieve robust obstacle avoidance in the dynamic condition. The comparison under the static condition is shown in Figure 7 from which we can observe that our method still performs more robustly than the existing methods.

B MORE EXPERIMENTAL SETTINGS

Implementation Details. The robot utilizes a Robo Peak Light Detection And Ranging (RPLIDAR) system as its sensing device to detect obstacles, offering a field of view of 180 degrees with 18 range measurements. Each topic subscribed from gazebo contains 18-dimensional Laser data and 5 frames (128×128) of DVS data that are continuous in time. The event frame is generated from the DVS events stream through Algorithm 3. EEM-SAN was trained in conjunction with a deep critic network. More implementation details and hyperparameter configurations for our EEM-SAN were shown in Table 6.

Algorithm 3 Converting events steam into event frame

Require: a stream of event $(e_t = (t, x, y, p)), t_n, W, H$

Initialize $s_n \leftarrow O_{H,W}$

Extract a subset of events $E \leftarrow \{e_y | t_{n-1} \leq \gamma \leq t_n\}$

Initialize $s_queue = (5, d_n)$

while event stream not stop **do**

for $e_t \in E$ **do**

$t, x, y, p \leftarrow e_t$

$s_n(x, y) \leftarrow |p|$

$s_queue.append(s_n)$

$s_queue.popleft()$

end for

end while

Table 6: Hyperparameter configurations.

Parameters	Values
Neurons per hidden layer for critic net	512,512,512
Actor learning rate	1e-4
Critic learning rate	1e-4
Reward discount factor	0.99
Maximum length of replay buffer	1e5

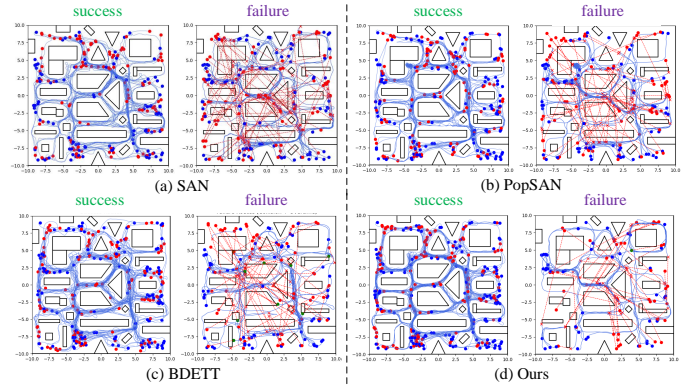


Figure 6: Success and failure trajectories of the four methods at the same 200 randomly sampled start and goal locations in dynamic condition. The blue dot represents the starting point, the red dot represents the target point, and the green dot represents the overtime case.

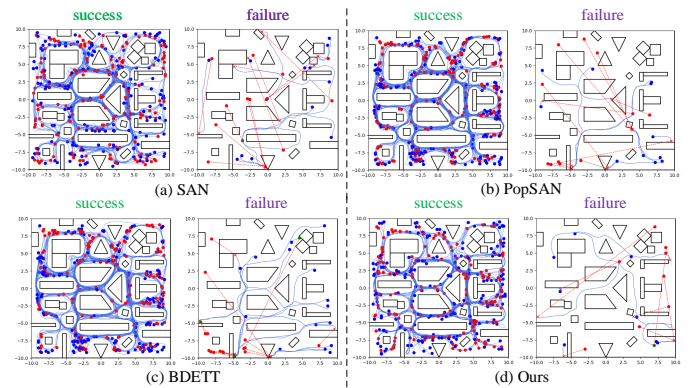


Figure 7: Success and failure trajectories of the four methods at the same 200 randomly sampled start and goal locations in static condition. The blue dot represents the starting point, the red dot represents the target point, and the green dot represents the overtime case.

Simulator Setup. During our training phase, we utilized the same form of curriculum training method as in SAN [43], which has been proven to result in better generalization and faster convergence [9].

For our evaluation phase, we assessed our method in the Gazebo simulator [19] within a $20m \times 20m$ test environment (Figure 8). The velocity of all moving obstacles within the test environment is listed in Table 7. To ensure comprehensive evaluation, we generated 200 start and goal locations, which were uniformly sampled at random from all parts of the test environment, with a minimum distance of $6m$. We used the same start and goal locations to evaluate our method, as well as all the compared methods (*i.e.*, SAN [43], PopSAN [44], and BDETT [7]).

Table 7: The speed of all dynamic obstacles in the evaluation environment.

Dynamic Obstacle	# 1	# 2	# 3	# 4	# 5	# 6	# 7	# 8	# 9	# 10	# 11
V_x (m/s)	1.4	1.4	1.4	1.2	0	0	0	1.4	1.3	1.4	0
V_y (m/s)	0	0	0	1.2	1.4	1.4	1.4	0	1.3	0	1.4

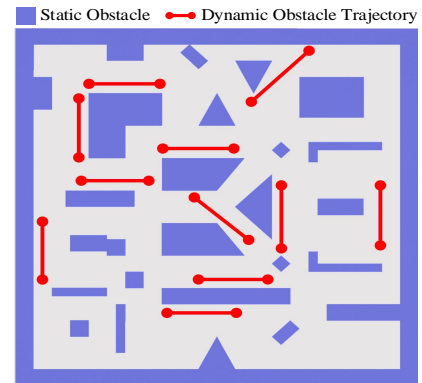


Figure 8: A testing environment containing both static and dynamic obstacles, with blue representing static obstacles of different shapes and red lines representing the movement trajectory of dynamic obstacles.